Design and Validation of a Compatible 3-Degrees of Freedom Shoulder Exoskeleton With an Adaptive Center of Rotation

Hua Yan
State Key Laboratory of Fluid Power Transmission and Control, Zhejiang University, Hangzhou 310027, China
e-mail: wereyh@zju.edu.cn

Canjun Yang[1]
State Key Laboratory of Fluid Power Transmission and Control, Zhejiang University, Hangzhou 310027, China
e-mail: ycj@zju.edu.cn

Yansong Zhang
State Key Laboratory of Fluid Power Transmission and Control, Zhejiang University, Hangzhou 310027, China
e-mail: zyansld@163.com

Yiqi Wang
State Key Laboratory of Fluid Power Transmission and Control, Zhejiang University, Hangzhou 310027, China
e-mail: jialeng@zju.edu.cn

This paper outlines an experimentally based design method for a compatible 3-DOF shoulder exoskeleton with an adaptive center of rotation (CoR) by matching the mechanical CoR with the anatomical CoR to reduce human–machine interaction forces and improve comfort during dynamic humeral motion. The spatial–temporal description for anatomical CoR motion is obtained via a specific experimental task conducted on six healthy subjects. The task is comprised of a static section and a dynamic section, both of which are recorded with an infrared motion capture system using body-attached markers. To reduce the influence of human soft tissues, a custom-made four-marker group block was placed on the upper arm instead of using discrete markers. In the static section, the position of anatomical CoR is kept stationary and calculated using a well-known functional method. Based on the static results, the dynamic section determines the statistical relationship between the dynamic CoR position and the humeral orientation using an optimization method when subjects move their upper arm freely in the sagittal and coronal planes. Based on the resolved anatomical CoR motion, a new mechanical CoR model derived from a traditional ball-and-socket joint is applied to match the experimental results as closely as possible. In this mechanical model, the CoR motion in three-dimensional space is adjusted by translating two of the three intersecting joint axes, including the shoulder abduction/adduction and flexion/extension. A set of optimal translation parameters is obtained through proper matching criterion for the two CoRs. Based on the translation parameters, a compatible shoulder exoskeleton was manufactured and compared with a traditional shoulder exoskeleton with a fixed CoR. An experimental test was conducted to validate the CoR motion adaptation ability by measuring the human–machine interaction force during passive shoulder joint motion. The results provide a promising direction for future anthropomorphic shoulder exoskeleton design.
[DOI: 10.1115/1.4027284]

Keywords: shoulder exoskeleton, center of rotation, adaptive, human–machine interaction force

1 Introduction

An anthropomorphic mechanical structure is one of the basic items required for exoskeleton robots to function properly, transfer useful motion patterns and avoid excessive interaction forces with the human body. A fundamental requirement of anthropomorphism is the alignment of the axis and/or CoR between the human and exoskeleton joints. The human shoulder joint is one of the most complex and flexible joints, containing a floating CoR due to the interplay of the glenohumeral joint and shoulder girdle [1]. A traditional 3-DOF ball-and-socket joint, that is usually adopted for the mechanical shoulder joint, has a fixed CoR that cannot mimic such a mechanism. However, most existing exoskeleton robots employ the traditional ball-and-socket joint as their shoulder joints [2–4], and the resulting misalignment of the mechanical and anatomical CoRs may lead to excessive human–machine interaction forces or even cause harm to the wearer [5]. To address this problem, this paper presents a compatible shoulder exoskeleton with an adaptive CoR derived from experimental data on anatomical CoR motion.

To design a self-adaptive mechanical shoulder exoskeleton robot, a thorough understanding and quantification of anatomical CoR motion is necessary and required to facilitate the anthropomorphic goal. As Fig. 1 shows, the shoulder joint comprises three bones, the humerus, the clavicle and the scapula, as well as four joints, the glenohumeral joint, the acromioclavicular joint, the scapulothoracic joint and the sternoclavicular joint [6]. The motion of the shoulder CoR plays a significant role in the description of the upper extremity kinematics [7], disease diagnosis [8], and arthroplasty [9]. Many methods for recording and describing the 3-D shoulder CoR motion have been previously presented. Poppen and Walker [10] obtained the relationship between the position of the anatomical CoR and the abduction angle in the plane of scapula from sequential roentgenograms of the shoulder joint on 12 normal subjects. However, the data were inadequate for shoulder exoskeleton design and the roentgenogram is not a desirable method because it requires radiation. Implantable sensors [11] can accurately monitor the orientation of the shoulder bones without the influence of soft tissues, but this approach is far too invasive, and has the potential for infection. Recently, motion capture systems using infrared cameras and reflective markers

[1]Corresponding author.
Contributed by the Mechanisms and Robotics Committee of ASME for publication in the Journal of Mechanical Design. Manuscript received February 4, 2013; final manuscript received March 19, 2014; published online April 28, 2014. Assoc. Editor: Matthew B. Parkinson.

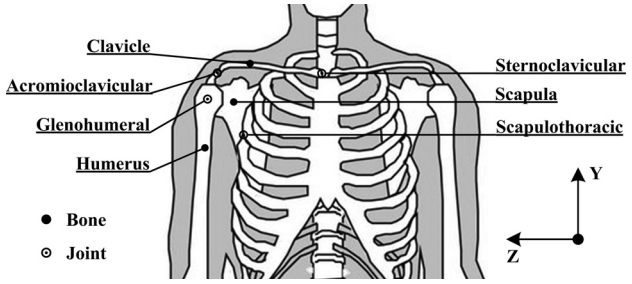

Fig. 1 Bones and joints of the shoulder complex

have attracted interest because of the harmless and precise description of both the dynamic limb motion and whole body movement. Thanks to the development of an infrared motion capture system, functional methods [12] can identify the position of the static joint CoR from a limited amount of relative motion in the adjacent limb, that is recorded using reflective markers. Lempereur et al. [13] compared the accuracy and repeatability of the functional methods, including the least squares solution [14], bias compensated [15], symmetrical center of rotation estimation [16], normalization method [17], and helical axis [18]. The least squares solution seems to have the best synthesized behavior in identifying the static CoR position of the ball-and-socket joint. Therefore, we designed an experimental task comprising two sections, a static and a dynamic section, to identify both the static and dynamic CoR motions. The static section adopts the functional method to calculate the position of the static CoR and the distance between the static CoR and a marker fixed on the upper arm. In the dynamic section, the upper arm moves freely in space, meaning that the functional method is not applicable to derive the dynamic motion of the shoulder CoR in real time. Therefore, for this experimental task, we used a specific optimization method based on the results of the static section to describe the dynamic CoR motion.

During the last decade, upper extremity exoskeleton robots have undergone extensive theoretical development for use in practical applications, including neuro-rehabilitation [19], power amplification [20], teleoperation [21], and virtual reality (VR) simulation [22]. Those exoskeleton robots realize their function by assisting and/or monitoring human arm movements through an anthropomorphic mechanical structure, which demands that the mechanical axis and/or CoR align in accordance with the anatomical joint axis and/or CoR, respectively. Due to the complexity of the anatomical shoulder joint, most exoskeleton robots available adopt a simplified joint model, such as the 3-DOF ball-and-socket joint to mimic shoulder joint motion. However, the ball-and-socket joint possesses a fixed CoR without any other supplementary passive or active joints. Therefore, the variable motion of the anatomical joint CoR during dynamic shoulder movement cannot be tracked when using such an over-simplified model. The mismatch between the mechanical and anatomical CoR results in the deformation of human soft tissues, forced movement of the human body and excessive interaction forces that must be avoided, especially during neuro-rehabilitation applications.

The designers of several upper extremity exoskeleton robots available have been aware of the importance of joint alignment and addressed this problem using different approaches. Among these devices, a majority of them use altered mechanical CoR positioning by adding one or more passive joints (Armeo [23], Dampace [24]), active joints (ARMin II [25], MGA [26], MEDARM [27]), or a combination of passive and active joints (IntelliArm [28]). The use of passive and/or active joints can simulate the motion of the shoulder complex entirely. Nevertheless, there is a compromise between system functionality, mechanical complexity, and expense. Additionally, extra joints will lead to control issues when operating all the exoskeleton joints simultaneously. As an alternative and more flexible means of handling this problem, ARMin III [29] obtained continuous motion data from an anatomical CoR as a function of the humerus elevation angle and human body size. These data were approximated with a radial arc as the mechanical shoulder CoR trajectory, that was performed by translating the elevation axis of the shoulder joint under a globe coordinate system (CS) [30]. Although this modified ball-and-socket joint was simple for implementation purposes, it only tracked the anatomical CoR motion for the limited amount of the radial arc in all the elevation planes. Therefore, the 3-D motion of an anatomical CoR cannot be completely mimicked using this mechanical shoulder model. This paper extends the mechanical shoulder model to fully cover the 3-D CoR motion by introducing a different coordinate system, the sagittal, frontal, transverse, and rotation (SFTR) system [31]. The new mechanical CoR motion in 3-D space is described by four translation parameters through two axes to calculate a set of optimized parameters by matching the two CoRs. Comparing with the globe model used in ARMin III [29], the new mechanical CoR model provides a more comprehensive treatment of the anatomical CoR motion. An anthropomorphic exoskeleton should transfer the exact force to complete the specified movements and should avoid excessive force caused by the misalignment of the axis and/or CoR [5]. Therefore, the interaction force during passive humeral motion was employed as the measurement of human–machine interaction compatibility in this paper.

In this research, a compatible 3-DOF shoulder exoskeleton based on experimental data taken from anatomical CoR motion is presented and validated. In Sec. 2, an experimental task comprising a static section and a dynamic section is described to quantify the dynamic motion of an anatomical CoR during free humeral movement. The new mechanical CoR model for a derived ball-and-socket joint due to the translation of the joint axes is presented in Sec. 3. Section 4 describes the implementation and validation of the compatible shoulder exoskeleton robot system followed by the conclusions.

2 Shoulder Joint Experimental Task

The shoulder joint experimental task, consisting of a static section and a dynamic section, is designed to obtain a spatial–temporal description of the anatomical CoR motion. The OptiTrack infrared motion capture system (NaturalPoint, Inc.) is employed in the task and six infrared cameras (V100:R2) are arranged in the semicircular pattern to record the position of markers placed on a human body. Figure 2 shows the location of seven reflective markers. One is placed on the Incisura Jugularis (IJ) as the origin for the body coordinate system and to record any potential torso swaying. Two markers located on the Lateral Epicondyle (EL) and the Medial Epicondyle (EM) are used to calculate the humeral orientation according to the International Society of Biomechanics (ISB) recommendations [6]. The remaining four markers are placed on the upper arm and are grouped as a block to minimize errors introduced by human soft tissues [32]. The structure and location of the marker block is optimized according to research by Camomilla et al. [12]. Therefore, the distances between each marker in the block are separated as far as possible and the block is placed significantly away from the shoulder CoR. Six healthy subjects (see Table 1) without any known shoulder disorders participated in the experimental task. Informed consent was obtained for all subjects.

2.1 Static Section. As the name suggests, the position of shoulder CoR is kept stationary during the static section. Therefore, the distance between the marker block and the CoR is constant by keeping the block in the same position and reducing the influence of the soft tissues. This setup has been previously determined to be reasonable through the testing of marker blocks [32]. Thus, the constant distance between the static CoR and each marker in the block is calculated through functional method [13]. The functional method is a well-known means to obtain the

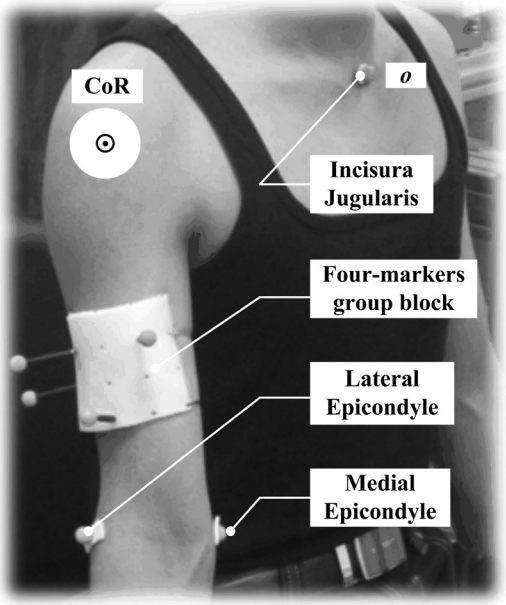

Fig. 2 Marker location on the human body

Table 1 Subject demographics

Rank	Age	Weight (kg)	Height (cm)	Arm length (mm)
1	24	62	174	550
2	20	60	172	551
3	24	56	168	475
4	31	56	173	540
5	26	59	171	494
6	26	70	172	518
	25.17 ± 3.6	60.5 ± 5.21	171.67 ± 2.07	521.33 ± 31.48

optimal CoR position for a human ball-and-socket joint, such as the shoulder joint or hip joint, through the functional movements of adjacent limbs, such as the humerus or thigh. Inman and Abbott [33] found an overall 2:1 relation between the humeral elevation and the scapular rotation. Considering that the distance between the CoR and the marker is much larger than the scapula length, the motion of the scapula is negligible when the humeral elevation angle is small. Therefore, the arc movement is found to be functional for both the flexion and abduction if their angles are less than 10 deg. The movement is performed at self-selected speeds. Different objective functions in the functional method were compared and validated by Camomilla et al. [12]. In this paper, the Spheric-4 (S4) algorithm [14] is applied for the static section due to its high precision and repeatability.

Figure 3 shows the implementation of the S4 algorithm using one marker on the upper arm and the global and body CS. The body CS *o-xyz* is established according to the ISB recommendations [6] with the origin *o* determined by the IJ marker and the *x-y-z* axes chosen to be in the frontal, upward and lateral directions, respectively. The global CS *O-XYZ* is defined by the motion capture system and the directions of the *X-Y-Z* axes are chosen to be the same as the body CS. Only the information from the IJ marker and the four block markers are used in the static section. The objective function of the S4 algorithm [14] is described by

$$f(\mathbf{m},\mathbf{r}^m)=\sum_{m=1}^{M}\sum_{n=1}^{N}\left[\left\|\mathbf{v}_n^m-\mathbf{m}\right\|^2-\left\|\mathbf{r}^m\right\|^2\right]^2 \tag{1}$$

All of the vectors are expressed in the global CS. The vector $\mathbf{v}_n^m$ points from the origin *o* to the marker block, where *M* is the

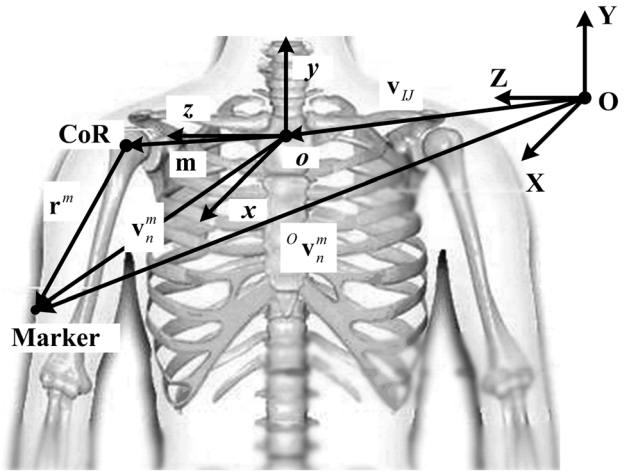

Fig. 3 Coordinate systems and vectors of one marker on an arm

Table 2 Mean distances and standard deviations between the four markers and the CoRs of six subjects (cm)

Rank	$\overline{r^1}$	$\overline{r^2}$	$\overline{r^3}$	$\overline{r^4}$
1	12.48(0.48)	18.11(0.68)	15.19(0.59)	11.27(0.73)
2	11.23(0.34)	16.29(0.75)	15.11(0.62)	10.56(0.58)
3	11.08(0.35)	15.71(0.64)	14.59(0.47)	10.24(0.63)
4	12.14(0.46)	16.73(0.59)	14.75(0.58)	11.14(0.61)
5	11.76(0.51)	17.37(0.54)	15.38(0.51)	11.23(0.71)
6	12.13(0.45)	16.49(0.48)	14.87(0.45)	11.36(0.54)

marker block number and *N* is the number of samples taken during the humeral arc movement. Here $M=4$ and $N=900$. The variable $\mathbf{v}_n^m$ can be calculated by $\mathbf{v}_n^m={}^O\mathbf{v}_n^m-\mathbf{v}_{\mathrm{IJ}}$. The vector ${}^O\mathbf{v}_n^m$ is the upper arm marker position and $\mathbf{v}_{\mathrm{IJ}}$ denotes the IJ marker vector, that compensates for errors introduced by unavoidable slight torso swaying during humeral motion. The variables $\mathbf{r}^m$ and $\mathbf{m}$ are vectors from the CoR to the marker and the origin *o* to the CoR, respectively. Differentiating Eq. (1) with respect to $\mathbf{m}$ and $\mathbf{r}^m$, respectively, yields

$$U\mathbf{m}=\mathbf{V} \tag{2}$$

where

$$U=2\sum_{m=1}^{M}\left[\frac{1}{N}\sum_{n=1}^{N}\mathbf{v}_n^m(\mathbf{v}_n^m)^T-\frac{1}{N}\sum_{n=1}^{N}\mathbf{v}_n^m\left(\frac{1}{N}\sum_{n=1}^{N}\mathbf{v}_n^m\right)^T\right] \tag{3}$$

and

$$\mathbf{V}=\sum_{m=1}^{M}\left[\frac{1}{N}\sum_{n=1}^{N}(\mathbf{v}_n^m)^3-\frac{1}{N}\sum_{n=1}^{N}\left[\mathbf{v}_n^m\frac{1}{N}\sum_{n=1}^{N}(\mathbf{v}_n^m)^2\right]\right] \tag{4}$$

Because the optimal CoR position $\mathbf{m}$ is obtained by Eq. (2), the mean distance between the CoR and block marker is obtained by

$$\overline{r^m}=\sqrt{\sum_{n=1}^{N}\left(\nu_n^m-\mathbf{m}\right)^2/N},\quad m=1,2,3,4 \tag{5}$$

Six subjects repeated the humeral arm movement five times, $\overline{r^m}$ ($m=1, 2, 3, 4$) and the corresponding standard deviations are displayed in Table 2. The results show good data consistency and will be further employed for the dynamic section.

2.2 Dynamic Section. Compared with the constant CoR used in the static section, the dynamic section encourages natural movements of the upper limb, that means no additional constraints are placed on the subject, and the humerus (the dynamic CoR) moves freely in space. Six subjects began the dynamic section with all the markers position unchanged and used the humerus for a lifting movement with the hand moving from the lowest point to the highest point in different elevation planes as the elbow joint is fully extended. Here the lifting movements in the sagittal and coronal planes are selected as an example to test our experimental task and further design methods due to its flexibility for implementation and validation of the subsequent mechanical CoR model. The movements are repeated five times at self-selected speeds and the mean result is recorded. The optimal CoR motion of the dynamic movements in the sagittal and coronal planes can be calculated using

$$f(\mathbf{m}) = \sum_{m=1}^{M} \left[\left\| \mathbf{v}_n^m - \mathbf{m} \right\|^2 - (r^m)^2 \right] \tag{6}$$

where $\overline{r^m}$ ($m = 1, 2, 3, 4$) for each marker is obtained in the static section and $\mathbf{v}_n^m$ is the marker vector obtained during the lifting movement. The number of samples is set to 900 for each flexion and abduction movement. Therefore, for a set of four markers position vector $\mathbf{v}_n^m$ ($m = 1, 2, 3, 4$ and $n = 1$–900), the optimal position of the CoR, $\mathbf{m}$, may be calculated by minimizing $f(\mathbf{m})$ for a specified humeral orientation. The Levenberg–Marquardt method [34] is used to solve this problem. The humeral orientation corresponding to each CoR position, such as the elevation angle in sagittal and coronal planes, is calculated by the two markers located on the EL and the EM according to

$$(x_\nu, y_\nu, z_\nu) = (\nu_{\mathrm{EL}} - \nu_{\mathrm{EM}})/2 - \mathbf{m} \tag{7}$$

where

$$\theta_{\mathrm{flex}} = \arccos\left(y_\nu / \sqrt{x_\nu^2 + y_\nu^2} \right) \tag{8}$$

$$\theta_{\mathrm{abd}} = \arccos\left(y_\nu / \sqrt{y_\nu^2 + z_\nu^2} \right) \tag{9}$$

The variables $\mathbf{v}_{\mathrm{EL}}$ and $\mathbf{v}_{\mathrm{EM}}$ describe the marker vectors placed on the EL and the EM, respectively. The variables θ_{flex} and θ_{abd} are the elevation angles in the sagittal and coronal planes, respectively. From this, the anatomical CoR position ($\mathbf{m}$), represented as (O_x, O_y, O_z), can be expressed as the function of the elevation angles (θ_{flex} and θ_{abd}). Figure 4 shows the mean anatomical CoR motion for the six subjects performing a humerus lifting movement in the sagittal and coronal planes, respectively, in a 3-D CS and in the X-, Y-, and Z-plane CS, whereas the CS of the three planes shows the additional minimum and maximum CoR positions for the six subjects involved in this experimental task. The elevation angle of abduction movement is restricted to be less than 150 deg because torso tilt occurs when the abduction angle becomes too large, which is beyond the scope of this research.

The CoR position for the same humeral orientation is supposed to be at the same location, meaning that the dynamic trajectory of the CoR position in different elevation planes should be curves with the same origin and endpoint. However, because the shoulder joint is unstable and redundant, it is impossible to maintain the same CoR position between different elevation movements. The obtained results confirm this point. Because of the individual difference in motor coordination and a lack of a large sample set, no obvious correlation was found between the CoR motion and human dimensions. The maximum, average, and minimum movements of the CoR are illustrated in Fig. 4. The flexion and abduction movements have the same CoR motion trends in the Y- and Z-directions, shown by the CoR moving upward and inward

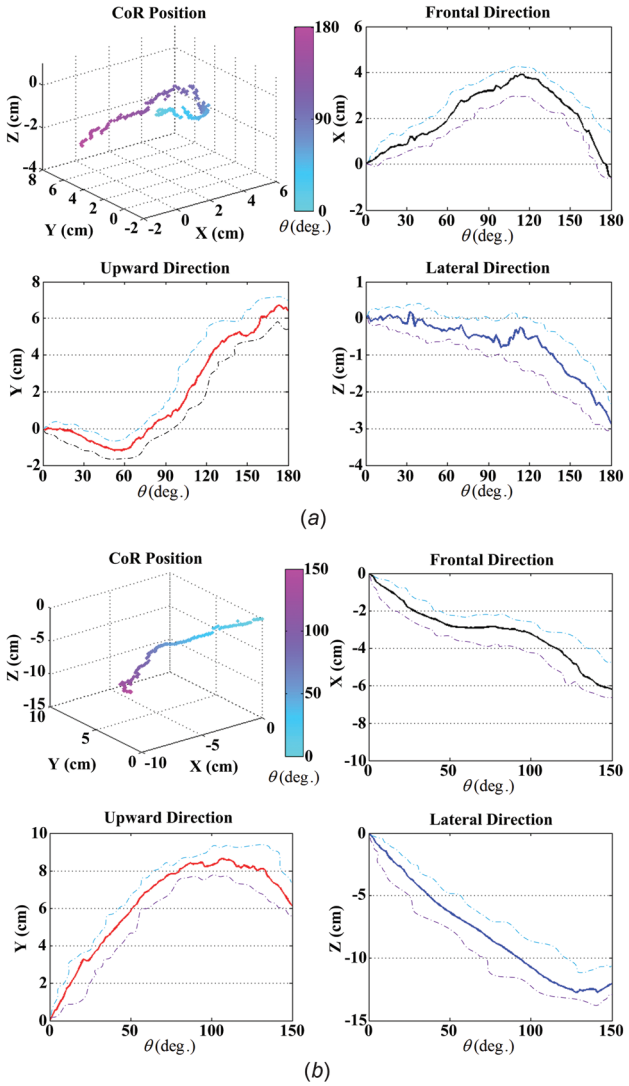

Fig. 4 Diagrams of the CoR position during humerus lifting movements in the sagittal plane (*a*) and coronal plane (*b*)

during the humerus lifting movement. However, there are differences in both the appearance and magnitude. During the flexion movement, the CoR stays in the same position up to slightly prior to 30 deg in the Y-direction before a small decrease appears and reaches a minimum value at 58.6 deg. Unlike the concave structure observed for the flexion movement, the abduction movement exhibits a convex curve with a maximum value observed at 113 deg. The decline afterward is attributed to the scapula tilt for shoulder comfort, that also causes the human torso to incline toward the medial direction. The maximum magnitudes in the Y-direction are 6.8 cm and 8.9 cm, during flexion and abduction, respectively. Both the flexion and abduction movements cause a decrease in the position in the Z-direction, whereas the abduction movement exhibits much more movement than flexion. As mentioned, this circumstance is due to scapula tilt coupled with a torso decline when the abduction angle is greater than 90 deg. A large difference in the appearance and magnitude is found in the X-direction between the flexion and abduction movements. The shoulder CoR moves forward until reaching a maximum value at 116 deg, before falling backward to the initial position. This is due to the features of flexion movement. However, a monotonous decrease in the CoR position is found in the X-direction during abduction movement. A reasonable explanation is that the

subjects are likely to move backward when lifting their humeri in the coronal plane. Subjects also approved this activity after the experimental task. Humeral internal/external rotation did not show a significant impact on the CoR position in our experimental task.

3 The Mechanical CoR Model

Traditional ball-and-socket joints contain a fixed CoR that is unable to mimic the anatomical CoR motion obtained in the previous experimental task. Therefore, a compatible shoulder exoskeleton needs to be designed with a mechanical CoR that corresponds to the anatomical one. ARMin III [29] provided a novel way to determine the alterable dynamic mechanical CoR by translating one axis, so that the motion of CoR forms a circular arc. The result showed a feasible and promising path toward an anthropomorphic and compact shoulder exoskeleton robot. Nevertheless, the single circular arc is inadequate to cover the spatial anatomical CoR motion that is shown in Fig. 4. Therefore, this paper extends the traditional ball-and-socket joint model to form mechanical CoR motions in the sagittal and coronal planes that coincide with the obtained anatomical CoR motions as much as possible.

First, there are two conventional systems that unambiguously describe the ball-and-socket joint behavior that needs to be introduced. One is the SFTR system [6], that measures the joint angles in the sagittal, frontal, and transverse planes. The other is the globe system [30], that describes the shoulder joint motion in terms of latitudes and longitudes on a globe in a specific sequence. ARMin III [29] adopts the globe system and determines a single circular arc by merely translating the elevation axis. This paper employs the alternative SFTR system and extends the mechanical CoR motion to 3-D space by translating two of the three rotation axes. Figure 5 shows the derivation process for the new mechanical model based on the SFTR system. The SFTR system comprises the X, Y, and Z axes that represent the axes for abduction/adduction, internal/external rotation and flexion/extension, respectively (see Fig. 5(*a*)). Obviously, the intersection point O remains stationary when joint rotation occurs. Here, the new CoR model is constructed by translating the abduction/adduction (X to X') and flexion/extension (Z to Z') axes. The translations are described in the Y-X and Y-Z planes using polar coordinates with the Y axis as the polar axis. The position of the new intersection points O_0 and O_1 can be expressed as

$$p_{O_0} = \rho_0 e^{i\alpha_0}$$

and

$$p_{O_1} = \rho_1 e^{i\alpha_1} \tag{10}$$

where ρ_0, ρ_1 and α_0, α_1 are the translation distances and angles with respect to the origin O and polar axis Y.

Using the new mechanical CoR model, the position of the CoR may be easily expressed by the translation parameters and the angles of the abduction and flexion movements. The rotation motion around the Z' axis followed by the X' axis (see Figs. 5(*b*) and 5(*c*), respectively) and the position of the CoR (point C) are shown in Fig. 5(*d*). This sequence of rotation is selected because the rotation around the distal Z' axis does not influence the position of the proximal X' axis due to the kinematic configuration of the SFTR system. The position of the new CoR point C is calculated by

$$\begin{cases} C_x = -\mathrm{Im}(A) \\ C_y = \mathrm{Re}(B) \\ C_z = \mathrm{Im}(B) \end{cases} \tag{11}$$

$$\text{where } A = \rho_1 e^{i\alpha_1} + \rho_1 e^{i(\pi+\alpha_1+\theta_{\text{flex}})} \tag{12}$$

$$B = \rho_0 e^{i\alpha_0} + \rho_0 e^{i(\pi+\alpha_0-\theta_{\text{abd}})} + \mathrm{Re}(A) e^{-i\theta_{\text{abd}}} \tag{13}$$

and θ_{abd}, θ_{flex} are the angles of abduction and flexion, respectively. When $\alpha_0 = 270$ deg, $\rho_0 = 1$ cm and $\alpha_1 = 90$ deg, $\rho_1 = 1$ cm, the position of the CoR (point C) is calculated by Eq. (11) and shown in Fig. 6(*a*). Figure 6(*b*) shows another circumstance when $\alpha_0 = 180$ deg, $\rho_0 = 1$ cm and $\alpha_1 = 135$ deg, $\rho_1 = 2$ cm. Several conclusions may be inferred to understand the new mechanical CoR

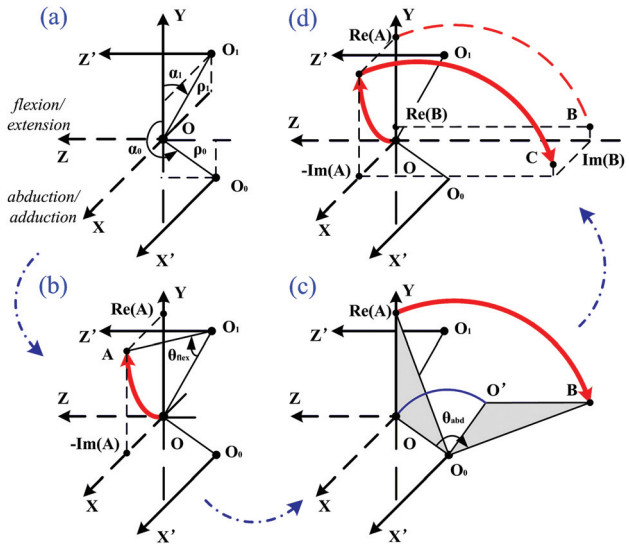

Fig. 5 (*a*) Translation of the axes for abduction/adduction (X) and flexion/extension (Z), (*b*) flexion around a new axis (Z'), (*c*) abduction around a new axis (X'), and (*d*) new CoR position C

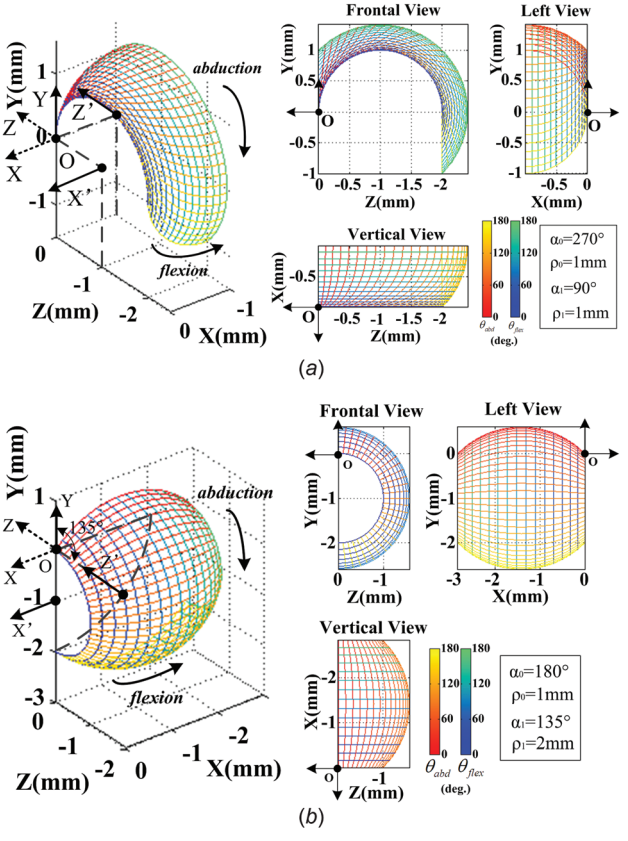

Fig. 6 Three-dimensional description of the mechanical CoR (point C) motion under different translation parameters. (*a*) $\alpha_0 = 270$ deg, $\rho_0 = 1$ cm and $\alpha_1 = 90$ deg, $\rho_1 = 1$ cm and (*b*) $\alpha_0 = 180$ deg, $\rho_0 = 1$ cm and $\alpha_1 = 135$ deg, $\rho_1 = 2$ cm.

model thoroughly and to facilitate the mechanical joint design by comparison of these two diagrams. In Fig. 6(*a*), the new X' axis moves in the medial direction and the Z' axis departs from the frontal direction. As a result, the CoR trajectory follows in the same direction and centralizes in the areas formed by planes perpendicular to the two axes (X' and Z'). Therefore, the directions of axial translation, α_0 and α_1, are determined by the anatomical CoR motion relative to the coordinate system *O-XYZ*. Correspondingly, the magnitude of the CoR surface determines the translation distance, ρ_0 and ρ_1.

4 Implementation and Experiment

With the anatomical and mechanical CoR motion obtained, a proper criterion to evaluate the compatibility of the two CoR motions must be defined to match them as closely as possible. Here, the root-mean-square (RMS) error between the two CoR motions is proposed to be

$$\bar{E} = \sqrt{\frac{1}{N}\sum_{i=1}^{N}\left[(O_{x_i} - C_{x_i})^2 + (O_{y_i} - C_{y_i})^2 + (O_{z_i} - C_{z_i})^2\right]} \quad (14)$$

where (O_x, O_y, O_z) and (C_x, C_y, C_z) are the positions of the anatomical and the mechanical CoRs under the same humeral orientation, respectively, and N is the number of samples taken in the humeral orientation, taken here to be 1800 for the two movements. The translation parameters are considered to be optimized when $\bar{E}$ is minimized. To find the minimum value of $\bar{E}$, the range of translation distances and angles, that are set from −10 cm to 10 cm and 0 deg to 360 deg, respectively, are examined at a step size of 0.01 cm and 0.1 deg, respectively. The result is a minimum value of $\bar{E} = 1.56$ cm at $\alpha_0 = 285.0$ deg, $\rho_0 = 4.43$ cm and $\alpha_1 = 306.2$ deg, $\rho_1 = 4.74$ cm, which are considered to be the optimal translation parameters for exoskeleton design. Figure 7 shows the mechanical CoR motion (shown as a grid) calculated using the optimal translation parameters ($\alpha_0 = 285.0$ deg, $\rho_0 = 4.43$ cm and $\alpha_1 = 306.2$ deg, $\rho_1 = 4.74$ cm) and the anatomical CoR motion (shown by red and blue lines) obtained in the experimental task. The RMS error is primarily caused by the CoR motion at large elevation angles. When the angle of humeral movement is small, the mechanical and anatomical CoRs agree very well. However, the deviation increases with the angle. Because the shoulder range of motion during activities of daily living is concentrated in the region where both the angles of flexion and abduction are less than 90 deg, the demands of an anthropomorphic mechanical CoR model are considered to be satisfactory.

A compatible shoulder exoskeleton was manufactured using the optimized translation parameters ($\rho_0 = 4.43$ cm, $\alpha_0 = 285.0$ deg and $\rho_1 = 4.74$ cm, $\alpha_1 = 306.2$ deg). As Fig. 8 shows the exoskeleton has three actuated DOFs, corresponding to adduction/abduction, flexion/extension, and internal/external rotation. The

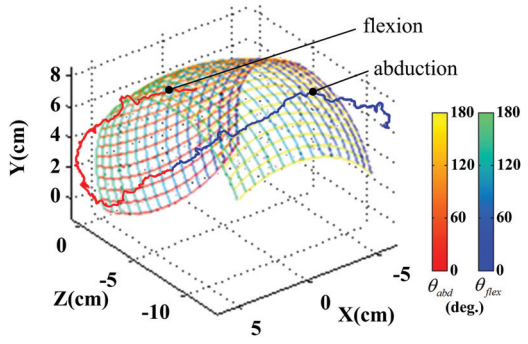

Fig. 7 Matching between the mechanical CoR motion (grid) calculated using the optimal translation parameters and the anatomical CoR motion (red and blue lines) obtained in the experimental task

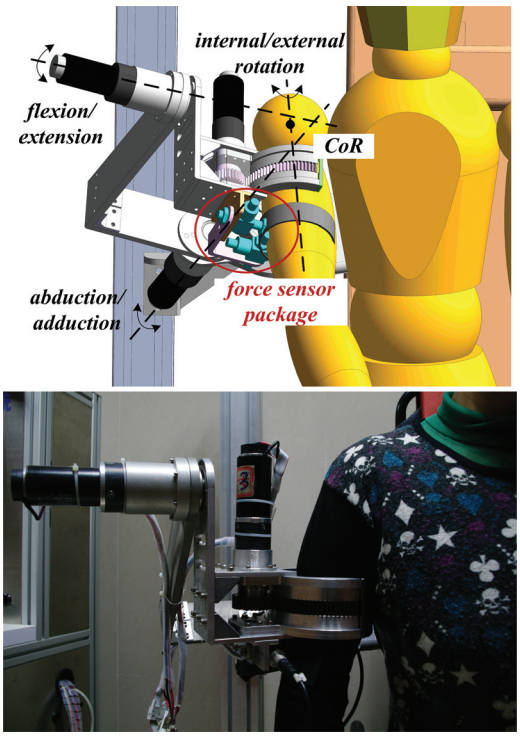

Fig. 8 Shoulder exoskeleton and subject in experimental test

Table 3 Specifications of the shoulder joint exoskeleton

Joint on exoskeleton	Joint range θ (deg)	Joint torque T (N·m)	Motor and gearbox
Abd./Add.	−100 to 60	20	RE40 + GPL52
Flex./Ext.	−60 to 180	20	RE40 + GPL52
Int./Ext. rotation	−80 to 90	12	RE40 + GPL42K

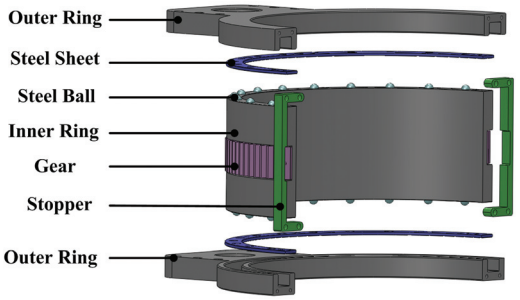

Fig. 9 Exploded view of the semi-circular guide rail

actuation unit combines the motor (Maxon Inc.) with gearbox (Gysin Inc.) and is mounted on each joint directly. The specifications for each joint are shown in Table 3. The internal/external rotation is performed using a custom-made semi-circular guide rail, as shown in Fig. 9. The orientation of the whole shoulder exoskeleton is altered to move the singularity to the boundary of the human workspace, that does not change the appearance and magnitude of mechanical CoR motion. Therefore, the two CoRs only need to be matched at the beginning of shoulder movement. The laser pointer is used to guarantee the accuracy of the CoR matching under the supervision of a skilled therapist. The interaction force is one of the most important issues, that is used to evaluate the comfort of human–machine physical interface [35]. A

Table 4 Subject demographics

Rank	Gender	Height (cm)	Weight (kg)	MRC Grade
1	Female	162	55	2
2	Female	156	49	1+
3	Female	168	65	2
4	Male	166	58	1+
5	Male	164	62	1+

mismatch between the human and the exoskeleton CoRs leads to excessive force, that may introduce deformation of the human soft tissues or forced motion upon the human body. These must be avoided, especially for exoskeleton robots used for neurorehabilitation. For these reasons, the interaction force at the human–machine physical interface of the newly designed shoulder exoskeleton and traditional exoskeleton owning a fixed CoR is examined. Two one-dimensional force sensors (see Fig. 8) are packaged together to measure the force of human–machine interaction in the sagittal and coronal planes, respectively.

Five post-stroke patients without any known shoulder disorders participated in the experimental test. Informed consent was obtained and the experimental procedure was approved and supervised by a skilled therapist. As shown in Table 4, patients with low Medical Research Council (MRC) grades [36] are chosen to minimize the active force exerted on the interaction port, so that the force sensors primarily examine the interaction force due to passive shoulder joint motion. Two movements are conducted by each subject, flexion and abduction at angles less than 90 deg. The joint speed is set at 15 deg/s. Only the force in the same plane is measured when the movement is performed. This corresponds to the force in the sagittal plane during flexion and the force in the coronal plane during abduction. Figure 10 shows the mean interaction forces on the five patients wearing the new and traditional shoulder exoskeletons during flexion and abduction movements. Both interaction forces increase when the abduction and flexion movements are performed, and tend to have the same maximum value, approximately 9 N on average, roughly the same as the effect of gravity on the human arm. A decrease in the interaction force during abduction and flexion movements, corresponding to 26.3% and 39.6%, respectively, at the maximum values, is observed when comparing the new exoskeleton with the traditional exoskeleton. However, several differences are observed. The reduction in the interaction force is more evident in flexion than abduction. Additionally, small elevation angles exhibit less interaction forces than large elevation angles. The results are interpreted to agree well and are in accordance with the CoR compatibility. As Fig. 7 shows, the mechanical CoR matches the anatomical CoR much better at small elevation angles. The flexion matching degree is better than abduction, that is indicated by the

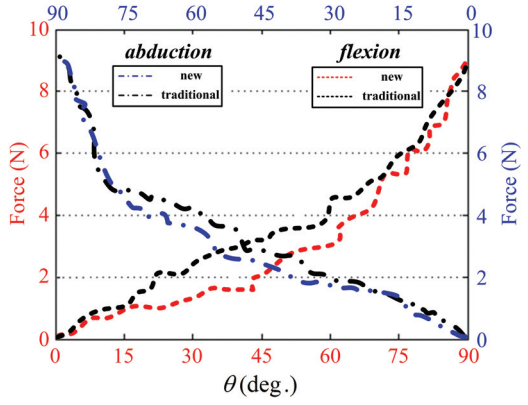

Fig. 10 Interaction force comparison between the new and traditional exoskeleton robots

RMS errors ($\overline{E}_{\text{flex}} = 1.03$ cm and $\overline{E}_{\text{abd}} = 1.43$ cm) of the corresponding movements. The results also confirm the research of Ref. [5] which describes that compatible structures decrease unnecessary forces due to the misalignment of the CoR and improves the comfort of human–machine interaction.

In addition to the interaction force, individual perception and electromyographic (EMG) signals have been considered as complementary metrics. A questionnaire was given to the five subjects after the experimental test. The subjects, who were uninformed about the specific types of exoskeleton robots, were asked to choose the more comfortable one after training on both the traditional and new robots. Two subjects chose the new one and the rest could not tell the differences between the two exoskeleton robots. However, individual perception is subjective and easily influenced by the unstable condition of patient. Additionally, the EMG signals do not adequately reflect the real status of muscles due to the nerve damage on the affected side. Therefore, interaction force is considered to be the most objective metric developed thus far.

5 Conclusions

To achieve a compatible human–machine physical interface, the design method presented proposes an anthropomorphic shoulder exoskeleton based on anatomical data to achieve agreement between the mechanical and anatomical shoulder CoRs during dynamic humeral motion.

The anatomical motion of the CoR is obtained from an experimental task composed of a static section and a dynamic section. The functional method [12] in the static section suffices to calculate the position of the constant CoR, but is powerless to address the dynamic CoR motion. Therefore, a dynamic section is added and the optimal position of the CoR during flexion/extension and abduction/adduction is obtained by minimizing a self-defined cost function. Compared with the use of sequential roentgenograms [10] and implantable sensors [11], the experimental task successfully obtained a precise quantification of the anatomical CoR motion, that greatly assisted the exoskeleton design.

Designing for compatibility of a mechanical shoulder CoR has been used by many exoskeleton robots available. Several devices solve this problem by adding one or more active/passive joints but introduce problems associated with bulky mechanisms and control issues [23–28]. ARMin III [29] provides an alternative method by translating one axis of the ball-and-socket joint. However, the derived CoR trajectory is a single circular arc in all the elevation planes, that is unable to cover the complex anatomical CoR motion thoroughly. In this research, a description of mechanical CoR motion is performed using the SFTR system [6] instead of the globe system used by ARMin III [29]. Two axes (flexion/extension and abduction/adduction) are translated to form a curved surface, that matches the positon of the anatomical CoR much better than the single circular arc. The RMS error of matching $\overline{E} = 1.56$ cm is low compared with the range of anatomical CoR motion (maximum value equaling 8–10 cm).

The new shoulder exoskeleton was validated by five post-stroke patients and compared with the traditional one. The clinical results indicated a more comfortable human–machine physical interface, as determined by the decrease in the interaction force of up to 39.6%. The improvement provides a more compatible and safer experience for shoulder exoskeleton robots without increasing the number of redundant joints. The compact structure can, also, be applied in other areas, such as virtual reality, to understand force transmission better.

The key results from our research are summarized as follows:

(1) The dynamic section based on the static CoR position is sufficient to obtain the dynamic CoR motion in 3-D space. The method may be used as a supplement of the functional method for shoulder function assessment and diagnosis.
(2) The mechanical CoR motion constructed by translating the axes of flexion/extension and adduction/abduction provides

an adequate matching to the anatomical CoR motion (RMS error $\overline{E} = 1.56$ cm).

(3) The interaction force between the human and the new anthropomorphic shoulder exoskeleton decreases compared to the traditional one, especially for angles of abduction and flexion less than 90 deg. The experimental results support the hypothesis that the interaction force decreases when the mechanical CoR moves with the rhythm of an anatomical one.

In the dynamic section, only the flexion and abduction movements are completed as an example to test the feasibility of our method. The next step will be to add more humeral movements to construct the whole range of anatomical CoR motion to design a more compatible shoulder exoskeleton suitable for the full range of shoulder motion. Additionally, the small subject size used in the experimental task and validation is limited and insufficient to obtain statistical results, that need be more convincing and adequate for the exoskeleton design. Therefore, subjects over a wide range of human dimensions must be examined to understand the characteristics of anatomical CoR motion thoroughly. Another improvement is the development of criteria for matching between the anatomical and mechanical CoRs. The adopted RMS criterion provides a global optimization that avoids a large deviation but along with local misalignment. Thus, the CoR area based criteria may be better for some specific CoR motion. This is another item we will examine as our project moves forward.

In conclusion, the experimental task provides a description of the dynamic anatomical CoR motion, that greatly facilitates our anthropomorphic design. The mechanical CoR model based on the SFTR system exhibits better coverage of the anatomical CoR motion, but a number of improvements are still needed to obtain a full matching range. The next steps in this research will address these problems.

Acknowledgment

The authors would like to thank the National Key Technology R&D Program by the National Science and Technology Ministry under Grant No. 2009BAI71B07 and Science Fund for Creative Research Groups of National Natural Science Foundation of China under Grant No. 51221004. Additionally, the authors would like to thank Donghai Wang and Qian Bi for providing suggestions regarding the experimental design.

Nomenclature

(C_x, C_y, C_z) = position of the mechanical CoR (cm)
$\overline{E}$ = root-mean-square error of the mechanical and anatomical CoR (cm)
$\mathbf{m}$ = vector from the IJ marker to the marker block (cm)
M = marker number
N = number of samples
(O_x, O_y, O_z) = position of the anatomical CoR (cm)
$\mathbf{r}^m$ = vector from the CoR to the marker in block (cm)
$\overline{r^m}$ = mean distance from the CoR to the marker in block (cm)
$\mathbf{v}_n^m$, ${}^O\mathbf{v}_n^m$ = vector from origin o and O to marker (cm)
$\mathbf{v}_{EL}$, $\mathbf{v}_{EM}$, $\mathbf{v}_{IJ}$ = vector from marker on EL, EM, and IJ (cm)

Greek Symbols

α_0, α_1 = translation angle of the rotation axis (deg)
ρ_0, ρ_1 = translation distance of the rotation axis (cm)
θ_{abd}, θ_{flex} = angle of abduction and flexion (deg)

References

[1] Hogfors, C., Peterson, B., Sigholm, G., and Herberts, P., 1991, "Biomechanical Model of the Human Shoulder Joint—II. The Shoulder Rhythm," J. Biomech., **24**(8), pp. 699–709.
[2] Perry, J. C., Rosen, J., and Burns, S., 2007, "Upper-Limb Powered Exoskeleton Desing," IEEE/ASME Trans. Mech., **12**(4), pp. 408–417.
[3] Sugar, T. G., He, J., Koeneman, E. J., Koeneman, J. B., Herman, R., Huang, H., Schultz, R. S., Herring, D., Wanberg, J., and Balasubramanian, S., 2007, "Design and Control of RUPERT: A Device for Robotic Upper Extremity Repetitive Therapy," IEEE Trans. Neural Syst. Rehabil. Eng., **15**(3), pp. 336–346.
[4] Caldwell, D. G., Tsagarakis, N., Kousidou, S., Costa, N., and Sarakoglou, I., 2007, "'Soft' Exoskeleton for Upper and Lower Body Rehabilitation–Design, Control, and Testing," Int. J. Hum. Rob., **4**(3), pp. 549–574.
[5] Schiele, A., and Van Der Helm, F. C. T., 2006, "Kinematic Design to Improve Ergonomics in Human Machine Interaction," IEEE Trans. Neural Syst. Rehabil. Eng., **14**(4), pp. 456–469.
[6] Wu, G., Van Der Helm, F. C. T., Veeger, H., Makhsous, M., Van Roy, P., Anglin, C., Nagels, J., Karduna, A. R., Mcquade, K., and Wang, X., 2005, "ISB Recommendation on Definitions of Joint Coordinate Systems of Various Joints for the Reporting of Human Joint Motion—Part II: Shoulder, Elbow, Wrist, and Hand," J. Biomech., **38**(5), pp. 981–992.
[7] Morrow, M. M. B., Kaufman, K. R., and An, K. N., 2011, "Scapula Kinematics and Associated Impingement Risk in Manual Wheelchair Users During Propulsion and a Weight Relief Lift," Clin. Biomech., **26**(4), pp. 352–357.
[8] Hingtgen, B., Mcguire, J. R., Wang, M., and Harris, G. F., 2006, "An Upper Extremity Kinematic Model for Evaluation of Hemiparetic Stroke," J. Biomech., **39**(4), pp. 681–688.
[9] Harryman, D. T., Sidles, J. A., Harris, S. L., Lippitt, S. B., and Matsen, F. A., 1995, "The Effect of Articular Conformity and the Size of the Humeral Head Component on Laxity and Motion after Glenohumeral Arthroplasty—A Study in Cadavera," J. Bone Jt. Surg. Am., **77**(4), pp. 555–563. Available at: http://jbjs.org/article.aspx?articleid=22935
[10] Poppen, N., and Walker, P., 1976, "Normal and Abnormal Motion of the Shoulder," J. Bone Jt. Surg. Am., **58**(2), pp. 195–201.
[11] Karduna, A. R., 2001, "Direct 3-Dimensional Measurement of Scapular Kinematics During Dynamic Movements in vivo," J. Shoulder Elbow Surg., **10**(3), pp. 269–277.
[12] Camomilla, V., Cereatti, A., Vannozzi, G., and Cappozzo, A., 2006, "An Optimized Protocol for Hip Joint Centre Determination Using the Functional Method," J. Biomech., **39**(6), pp. 1096–1106.
[13] Lempereur, M., Leboeuf, F., Brochard, S., Rousset, J., Burdin, V., and Rémy-Néris, O., 2010, "In vivo Estimation of the Glenohumeral Joint Centre by Functional Methods: Accuracy and Repeatability Assessment," J. Biomech., **43**(2), pp. 370–374.
[14] Gamage, S. S., and Lasenby, J., 2002, "New Least Squares Solutions for Estimating the Average Centre of Rotation and the Axis of Rotation," J. Biomech., **35**(1), pp. 87–93.
[15] Halvorsen, K., 2003, "Bias Compensated Least Squares Estimate of the Center of Rotation," J. Biomech., **36**(7), pp. 999–1008.
[16] Ehrig, R. M., Taylor, W. R., Duda, G. N., and Heller, M. O., 2006, "A Survey of Formal Methods for Determining the Centre of Rotation of Ball Joints," J. Biomech., **39**(15), pp. 2798–2809.
[17] Chang, J. H., Hsu, A. T., and Chang, G. L., 2008, "In vitro Estimation of Glenohumeral Joint Center of Rotation," J. Med. Biol. Eng., **28**(4), pp. 191–195. Available at: http://jmbe.bme.ncku.edu.tw/index.php/bme/article/viewArticle/306
[18] Woltring, H., Huiskes, R., De Lange, A., and Veldpaus, F., 1985, "Finite Centroid and Helical Axis Estimation From Noisy Landmark Measurements in the Study of Human Joint Kinematics," J. Biomech., **18**(5), pp. 379–389.
[19] Frisoli, A., Salsedo, F., Bergamasco, M., Rossi, B., and Carboncini, M. C., 2009, "A Force-Feedback Exoskeleton for Upper-Limb Rehabilitation in Virtual Reality," Appl. Bionics Biomech., **6**(2), pp. 115–126.
[20] Kobayashi, H., Suzuki, H., Iba, M., and Hasegawa, S., 2006, "Development of a Shoulder Mechanism for a Muscle Suit Supporting Upper Limb Motion and Proposal of a Posture Control Method," Trans. Soc. Instrum. Control Eng., **42**(4), pp. 376–385. Available at: https://www.jstage.jst.go.jp/article/sicetr1965/42/4/42_4_376/_article
[21] Zhang, J., Fu, H., Dong, Y., Zhang, Y., Yang, C., and Chen, Y., 2008, "Novel 6-DOF Wearable Exoskeleton Arm With Pneumatic Force-Feedback for Bilateral Teleoperation," Chin. J. Mech. Eng., **21**(3), pp. 58–65.
[22] Mihelj, M., Nef, T., and Riener, R., 2007, "A Novel Paradigm for Patient-Cooperative Control of Upper-Limb Rehabilitation Robots," Adv. Rob., **21**(8), pp. 843–867.
[23] Gijbels, D., Lamers, I., Kerkhofs, L., Alders, G., Knippenberg, E., and Feys, P., 2011, "The Armeo Spring as Training Tool to Improve Upper Limb Functionality in Multiple Sclerosis: A Pilot Study," J. Neuroeng. Rehabil., **8**(5), pp. 223–230.
[24] Stienen, A. H. A., Hekman, E. E. G., Van Der Helm, F. C. T., and Van Der Kooij, H., 2009, "Self-Aligning Exoskeleton Axes Through Decoupling of Joint Rotations and Translations," IEEE Trans. Rob., **25**(3), pp. 628–633.
[25] Mihelj, M., Nef, T., and Riener, R., 2007, "ARMin II–7 DoF Rehabilitation Robot: Mechanics and Kinematics," IEEE International Conference on Robotics and Automation, Roma, pp. 4120–4125.
[26] Carignan, C., Tang, J., and Roderick, S., 2009, "Development of an Exoskeleton Haptic Interface for Virtual Task Training," Proceedings of the IEEE/RSJ International Conference on Intelligent Robots and Systems, St. Louis, pp. 3697–3702.
[27] Ball, S. J., Brown, I. E., and Scott, S. H., 2007, "Medarm: A Rehabilitation Robot With 5DOF at the Shoulder Complex," IEEE/ASME International Conference on Advanced Intelligent Mechatronics, ETH Zurich, pp. 1–6.

[28] Park, H. S., Ren, Y., and Zhang, L. Q., 2008, "Intelliarm: An Exoskeleton for Diagnosis and Treatment of Patients With Neurological Impairments," Proceedings of 2008 IEEE RAS-EMBS International Conference on Biomedical Robotics and Biomechatronics, Scottsdale, pp. 109–114.
[29] Nef, T., Guidali, M., and Riener, R., 2009, "ARMin III–Arm Therapy Exoskeleton With an Ergonomic Shoulder Actuation," Appl. Bionics Biomech., **6**(2), pp. 127–142.
[30] Doorenbosch, C. A. M., Harlaar, J., and Veeger, D., 2003, "The Globe System: An Unambiguous Description of Shoulder Positions in Daily Life Movements," J. Rehabil. Res. Dev., **40**(2), pp. 147–156.
[31] Cave, E. F., and Roberts, S. M., 1936, "A Method for Measuring and Recording Joint Function," J. Bone Jt. Surg., **18**(2), pp. 455–465. Available at: http://jbjs.org/article.aspx?articleid=8431
[32] Gao, B., Conrad, B., and Zheng, N., 2007, "Comparison of Skin Error Reduction Techniques for Skeletal Motion Analysis," J. Biomech., **40**(2), pp. 551–551.
[33] Inman, V. T., and Abbott, L. R. C., 1944, "Observations on the Function of the Shoulder Joint," J. Bone Jt. Surg. Am., **26**(1), pp. 1–30. Available at: http://jbjs.org/article.aspx?articleid=10010
[34] More, J., 1978, "The Levenberg-Marquardt Algorithm: Implementation and Theory," Numer. Anal., **630**, pp. 105–116.
[35] Lenzi, T., Vitiello, N., Rossi, S. M. M. D., Persichetti, A., Giovacchini, F., Roccella, S., Vecchi, F., and Carrozza, M. C., 2011, "Measuring Human–Robot Interaction on Wearable Robots: A Distributed Approach," Mechatronics, **21**(6), pp. 1123–1131.
[36] Medical Research Council, 1976, *Aids to the Examination of the Peripheral Nervous System*, HMSO, London.